

Review : finite element analysis of stress transfer in short-fibre composite materials

K. L. Goh¹, R. M. Aspden², D. W. L. Hukins³

¹ *Biomaterials Division, Department of Optometry & Vision Sciences, Cardiff University, Redwood Building, King Edward VII Ave, Cathays Park, Wales, CF10 3NB, UK.*

² *Department of Orthopaedic Surgery, University of Aberdeen, Foresterhill, Aberdeen AB25 2ZD, UK.*

³ *School of Engineering, Mechanical Engineering, University of Birmingham, Edgbaston, Birmingham B15 2TT, UK.*

Correspondence: Dr K. L. Goh

Telephone: 029 20870204

Fax: 029 20874859

E-mail: gohk@cf.ac.uk

Abstract:

This paper addresses the application of finite element (FE) analysis for understanding the various processes that can occur and contribute to stress transfer between the matrix and fibres in short-fibre composite materials. These processes are elastic stress transfer, plastic stress transfer, matrix yielding (mode α), interfacial debonding (mode β), matrix cracking (mode γ), fibre pull-out and fibre fragmentation. In this paper, the discussion will cover the theory underlying each process, description of FE models, and analysis of stress transfer.

(79 words)

Key words: (A) short fibre composites, (B) fibre/matrix bond, (C) elastic properties, (C) stress transfer, (C) finite element analysis

1 Introduction

In general, the stress-strain curve characterizing a short-fibre composite material, when strained in tension parallel to a fibre direction, consists of four stages [1,2]. These stages are (1) elastic deformation of fibres and the matrix; (2) plastic deformation of the matrix whilst the fibres deform elastically; (3) plastic deformation of fibres and the matrix and (4) fracture of fibres followed by fracture of the composite material.

This paper addresses the application of finite element (FE) analysis for understanding the various processes that can occur during the four stages and contribute to stress transfer between the matrix and fibres in short-fibre composite materials. To date, the processes that have been studied by FE analysis are elastic stress transfer, plastic stress transfer, matrix yielding (mode α), interfacial debonding (mode β), matrix cracking (mode γ), fibre pull-out and fibre fragmentation. These processes are involved in the four stages as follows. In stage 1, elastic stress transfer occurs from an elastic matrix to an elastic fibre between a bonded interface during initial loading. During stage 2, the deforming matrix adjacent to the bonded interface may yield and become plastic (mode α). When debonding occurs at the fibre-matrix interface (mode β), sliding of the matrix over the fibre results in frictional stress transfer. If frictional stress transfer occurs at the interface adjacent to the deforming plastic matrix, then the combination of mode α and β lead to plastic stress transfer. Cracks may also occur in the matrix from the debonded fibre ends (mode γ). It follows that the combination of mode β and γ may lead to fibre pull-out; in the absence of mode β , if the cracks propagate to neighbouring intact fibres, then these neighbouring fibres become responsible for bridging the matrix cracks and hence fibre

pull-out still occurs. During stage 4, fibre fragmentation may occur in fibres that are bridging cracks in the matrix. Subsequently, the entire composite material fractures. Many fibre composite materials consist of brittle fibres in a ductile matrix. Since composites with brittle fibres fracture at the fracture strain of the fibre, it follows that stage 3 is not then observed [1,2].

The remainder of the paper consists of four main sections. Section 2 presents an overview of the models for studying the processes of stress transfer. Section 3 focuses on the contributions of the various stress transfer processes to a deforming fibre composite material. Section 4 presents the conclusions of this paper. Throughout this paper, we shall also highlight insights gained from understanding the response of stresses in the model to variation in material and geometric properties which would not be gained from an analysis that relies on specific values [3,4,5,6].

The following symbols used repeatedly throughout this paper are now explained. They refer to a model in which the composite consists of a single fibre surrounded by a coaxial cylinder of matrix. For fibres, we have the fibre axial ratio, $q (= L/r_o)$; here L and r_o are the half-length of the fibre and the radius at the center of the fibre, respectively. L_m and r_m denote the half-length and radius of the matrix, respectively. For material properties, we have E_f , E_m , ν_f and ν_m . Here, E and ν denote Young's modulus and Poisson's ratio, respectively; subscripts f and m in these symbols refer to the fibre and matrix, respectively. We also have σ_u , σ_y and τ_y ; these refer to the fibre fracture stress, matrix tensile yield stress and interfacial yield stress in shear, respectively; a Coulomb frictional model enables τ_y to be related to the coefficient of static friction, μ , and to the normal

(perpendicular) pressure, N [7]. Stress components, σ_z and τ , denote the fibre axial stress and interfacial shear stress; σ_c denotes the applied tensile stress in the direction of the fibre axis. Stress distributions are described with respect to the distance along the fibre axis, $Z (= z/L)$; here, z is the axial coordinate of the cylindrical polar coordinate system.

2 Description of models

2.1 Overview

Models for studying stress transfer in fibre composite materials can be grouped into two basic designs. The first is illustrated in Figure 1 which shows an axisymmetric FE model of a cylindrical fibre embedded in a cylindrical matrix [8,9,10,11,12,13]. The second design is similar to the first except that DEF'C (Figure 1) has been excluded [14,15,16,17,18,19]. In both designs, the axis of symmetry defines the z-axis of the cylindrical polar coordinate system. In many studies, the center of the model defines the origin of the coordinate system; for exceptions see Rauchs et al. [17] (section 2.6) and fibre pull-out models (section 2.7). In some studies, an annulus and an outer layer of material were introduced to describe fibre coating [16] and average composite properties [19], respectively; for the mathematical theory leading to these models, see Rosen [20].

It then follows that models for studying stress transfer processes are derived from one of these two basic designs and are distinguished by having different boundary conditions.

Axisymmetry is implemented by constraining OD (Figure 1). In many models mirror-symmetry is implemented by constraining OB (Figure 1). However, mirror symmetry along OB cannot be invoked for fibre pull-out models (section 2.7) or when the origin of

the coordinate system is not at the centre of the fibre [17] (see also section 2.6). It followed that models which featured mirror and axisymmetry are loaded in tension by prescribing an applied tensile force acting at CD in the direction of the fibre (Figure 1) or, in the case of the second basic design, at FF'; alternatively, these may be replaced by prescribing displacement. For a discussion of loading approaches for models in which mirror symmetry cannot be invoked, e.g. fibre pull-out models, or when the origin of the coordinate system is not at the center of the fibre see section 2.7 and 2.6, respectively.

The model shown in Figure 1 can also be modified to investigate stress transfer to fibres which are non-cylindrical in shape [10,21]. Revolution of the model about OD produces a half fibre which possess a conical, paraboloidal or ellipsoidal shape. These models were prompted by observations of taper at the ends of collagen fibrils in connective tissues [22,23] but the results are also applicable to synthetic fibre composite materials. In this paper, all results are for the cylindrical fibre study unless otherwise stated.

In the model shown in Figure 1, values assigned to r_m and L_m are determined by a 'far-field' analysis to ensure that any edge effects, i.e. arising from BC and CD, do not perturb the stresses in the fibre [8,10,11,15,24]. Note that the term 'far-field' has also been used for analytical studies of stress in fibre composite materials [25,26]. For the model described in Figure 1, it follows that by increasing r_m/r_o , stress distributions converge (Figure 2) and eventually one arrives at a sufficiently large matrix which is equivalent to an infinite matrix. Note that varying L_m/L has little effect on stresses along the fibre and across CD. Thus, the value of r_m/r_o at convergence corresponds to a model which is then useful for FE analysis.

2.2 Elastic stress transfer

The elastic stress transfer process involves the transfer of stress from an elastic matrix to an elastic fibre via a bonded interface. This predominates during initial loading (stage 1).

Bonding between the fibre and matrix, which is an important factor influencing the overall material properties of a fibre composite material [27], is imposed by node-sharing along the interface, AF. The assumption of an unbonded fibre end has been adopted as in Cox's theory [28]; physically, this has little effect on the overall stress distribution because of the small area of fibre which could adhere to the matrix [8].

In a typical FE analysis [8,10,11], the fibre and matrix materials are assumed to be isotropic. For an elastic material that is isotropic, it follows that out of a total of twenty-one material constants, only two are independent, i.e., E and ν [29]. Hence, the material constants to be considered in the FE analysis are the Young's moduli and Poisson's ratios of the fibre and matrix.

It is convenient to compare the effects of E_f and E_m on stresses together as a ratio of moduli, E_f/E_m ; E_f/E_m quantifies the elastic mismatch between a fibre and a matrix. A sensitivity analysis on varying E_f/E_m showed that increasing E_f/E_m (from 50 to 10000) for a fixed value of q (200 and 1000) had little effect on the shape of the stress distribution along the fibre axis [9]. Stress transfer between the matrix and fibre was more effective for larger values of E_f/E_m as this resulted in greater values for σ_z/σ_c , the stress produced in the fibre by a given applied stress. However, the presence of high stresses may lead to an increased risk of fibre fracture, i.e. when the maximum value of σ_z reaches the fibre fracture stress (section 2.8, 3.1, 3.6). The magnitude of the axial stress in the fibre is

much less sensitive to changes in q , and, as before, the stress distributions are all very similar [10]. Poisson's ratios, ν_f and ν_m , are often specified as single values [8,15]; they have negligible effect on the stresses in the model [10]. Although the effects of E_f/E_m , ν_f and ν_m were demonstrated for a cylindrical fibre [10], similar trends were also observed with tapered fibres [30].

2.3 *Matrix yielding (mode α)*

Mode α is said to occur when the deforming matrix yields and turns plastic adjacent to the bonded interface. In the case of uniform cylindrical fibres, stress concentrations in the matrix around the end, EF (Figure 1) [11] may lead to matrix yielding; for tapered fibres the lower stress concentrations in the matrix around the ends [31] may make them less susceptible to mode α . Results from an experiment suggested that stress distributions at the ends of a carbon fibre embedded in an epoxy matrix can be attributed to mode α [12].

In a typical FE model described by Figure 1, the matrix is modeled as an elastic-plastic material [11,12,16], i.e. the stress-strain curve is characterized by an initial (elastic) region described by a rapidly increasing stress with increasing strain and followed by a plastic region, described by little or no increase in stress with increasing strain [32]. The change from elastic to plastic properties at any point in the deforming matrix may be determined by comparing the stress state with σ_y [16]; by applying incremental displacements to the model, the change takes effect if the stress state exceeds σ_y .

2.4 *Matrix cracking (mode γ)*

Mode γ is said to occur when a crack at the debonded fibre end, EF (Figure 1), propagates into the matrix but not along the fibre-matrix interface [13]. A mode I crack, i.e. parting of two surfaces, implies that stress transfer will not occur across the crack planes and subsequently reduces the effectiveness of stress transfer between the matrix and fibre; a mode II crack, i.e. shear failure, enables stress transfer via friction at the crack surfaces [12]. It has been suggested [13] that matrix cracks described in experiments on carbon fibres embedded in epoxy matrix materials [33,34] are attributed to mode γ .

A modified Rice and Tracey micro-void nucleation, growth and coalescence model was used to predict the crack propagation in an FE analysis [13]. The model accounts for how a matrix crack is formed and how the crack propagates owing to voids present in the region ahead of the crack which nucleate, grow and coalesce due to the presence of high stress at the fibre corner. The modeling process was implemented by considering the matrix as an elastic-plastic material (section 2.3) and, under incremental displacement applied to the model at CD (Figure 1), the deforming matrix changes from elastic to plastic. A critical fracture strain was defined which depends on the void size and the stresses around the region. If the strain state at a point in the matrix was greater than this critical fracture strain then a crack was considered to have formed.

2.5 *Interfacial debonding (mode β)*

Mode β is said to occur when a crack initiates in the interface at the debonded fibre end, EF (Figure 1), and propagates along the interface, AF; frictional stress transfer occurs as

the deforming matrix slides over the fibre surface [12]. It has been pointed out that there is a relationship between the rate of debonding and E_f/E_m : the greater the E_f/E_m , the higher the rate of failure [9]. This implies that the greater the elastic mismatch between the fibre and matrix the higher the rate of interfacial failure. Interfacial debonding observed in experiments on carbon fibre embedded in epoxy matrix material, measured using laser Raman spectroscopy [33], have been attributed to mode β [26].

FE modeling on debonding and sliding at the fibre-matrix interface has been well documented [9,12,17]. Typically this has been implemented using a Coulomb friction model [12]. A model of this kind describes the increase in τ (to the value τ_y), as a result of an incremental load, when there is bonding at the fibre-matrix interface. Here τ_y depends on the frictional stress, μN , and a cohesive sliding resistance. When τ exceeds τ_y the two surfaces are deemed to have ‘debonded’ and will slide relative to one another when deformed further; this is referred to as the ‘sliding’ state. During the sliding state, the value of τ is constant throughout the interface; Rauchs et al. [17] have assigned $\tau = \tau_y$; clearly τ during sliding would be related to kinetic frictional stress and would thus be smaller than τ_y , which is related to static frictional stress.

2.6 *Plastic stress transfer*

Simultaneous occurrence of mode β and α at the interface, AF (Figure 1), and in the adjoining matrix region, respectively, leads to plastic stress transfer. Plastic stress transfer has been reported in mechanical test experiments combined with x-ray strain measurements using synchrotron radiation [17] or Raman spectroscopy [12].

Goh et al. [21] have considered an FE model consisting of an elastic fibre in tension under the application of a constant shear stress, τ , on its surface. This study showed that τ also acts as a scaling constant for σ_z ; this is consistent with the constant shear model of Kelly & Tyson [36].

In contrast, Rauchs et al. [17] considered an FE model consisting of an elastic-plastic matrix in which an elastic fibre of the same length as the matrix was embedded. This model corresponds to the second basic design described in section 2.1; in this case, the load in the direction of the fibre was applied through a prescribed axial displacement at EF' while OB was constrained to ensure no axial displacement could take place along it. This model represented conditions similar to an experiment that was conducted to study fibre fragmentation. By making assumptions about the different steps through which the modeling process should proceed (section 2.8), predictions from the model were compared with results obtained from experiment to yield an understanding about the stress transfer processes that took place. These steps progress from elastic stress transfer, mode α , β and finally to plastic stress transfer. Thereafter, the implementation of fibre fragments made it possible to analyse the stress distributions in short fibres as a consequence of plastic stress transfer.

It is useful to have an estimate of τ which may provide some information about the interfacial strength [35]. In the study carried out by Rauchs et al. [17], when mode β occurred, the value of τ was assigned equal to τ_y (section 2.5). It follows that the value of τ could be derived from $\tau_y = [E_f r_o / 2] d\varepsilon_z / dz$, adapted from the constant shear model of

Kelly & Tyson [36]; here, the fibre axial strain gradient, $d\varepsilon_z/dz$, is derived from the strain distribution curve obtained experimentally [17].

2.7 Fibre pull-out

Fibre pull-out may occur when fibres are drawn out from the faces of a matrix crack. In section 1, it was pointed that this may arise from the combination of modes β and γ ; in the absence of mode β , the matrix crack arising from mode γ may propagate to neighbouring fibres so that these fibres are responsible for bridging cracks in the matrix and hence fibre pull-out may also occur. The ability of a fibre to bridge a matrix crack depends on the interface (section 2.2), the fibre strength and fibre modulus [22]. If bonding is present at the interface, then the ability of a fibre to bridge the crack depends on τ_i ; if debonding has occurred, then this depends on friction as a result of sliding [27,37]. There are two possible outcomes of fibre pull-out arising from fibres bridging a matrix crack and they may also occur in combination [27]. The first is that matrix crack propagation is ‘deflected’ by the fibre and is led to propagate along the interface (mode β); the second is that the fibre fractures when attempts to bridge the crack causes it to be stressed beyond its fracture stress (section 2.8). Fibre pull-out has been observed in mechanical tests on synthetic materials [27,38] and in biological tissues [39].

The bridging of fibres across a crack to enable stress transfer can be investigated by fibre pull-out tests [37]; these tests are intended also to study the strength of the interface as a result of bonding and to investigate friction arising from sites where debonding has occurred [27]. A typical FE analysis [18] on fibre pull-out can be implemented by using the second basic design described in section 2.1 by loading the fibre at OA (Figure 1). In

order to model a matrix crack plane, AB is not constrained. In addition, FF' is then constrained to ensure no axial displacement can take place along it.

2.8 *Fibre fragmentation*

During the process of deformation, stress transfer from the matrix to a fibre may cause the fibre to break at the site where the fracture stress is attained. Fragments are generated by this process. It eventually stops when the fragments are so short (less than the critical length) that the mid-lengths of the fibre fragments fail to reach σ_u , i.e. not enough stress can be transferred to the fibre fragment to cause further fragmentation [17,40]. Fibre fragmentation has been observed in several experiments [33,41,42].

Rauchs et al. [17] performed an FE analysis to investigate the stresses in fibre fragments using the model described in section 2.6. Cracks were introduced at locations along the fibre by an element removal technique; the locations of these cracks were based on experimental results. The modeling process was divided into four steps. The first step corresponded to elastic fibre deformation; here the matrix changes from elastic to plastic during deformation, i.e. initially mode α , and subsequently, when mode β occurs, plastic stress transfer takes effect. Thereafter, the other steps involve mainly increasing the number of fragments in accordance with the sequence observed experimentally.

3 Stress transfer analysis

3.1 Elastic stress transfer

Figure 3 shows how the axial tensile stress in a cylindrical fibre, σ_z/σ_c , depends on E_f/E_m and q ; this result is taken from our previous work [10] but similar results, at restricted values for E_f/E_m and q , had been published previously [8,11]. In all cases, σ_z/σ_c is greatest at the centre of the fibre and decreases non-linearly to zero at its end. A similar dependence is predicted by shear lag models [11,28] and it has been shown that the predictions of FE and shear lag models are closely similar [10,11]. Similar results are also obtained experimentally [44]. Note that changing q has little effect on σ_z/σ_c .

A similar FE analysis has also been applied to non-cylindrical fibres [10]. In complete contrast to the cylindrical case, axial stress in a fibre with a conical taper is a minimum at the fibre centre; the stress rises and peaks near the fibre end before dropping to zero at the end. Stress distributions in ellipsoidal and paraboloidal fibres lie between the extremes of the cylinder and cone, leading to more uniform stress distributions. For low values of E_f/E_m (around 50), the stress distributions in conical, ellipsoidal and paraboloidal fibres are very similar and there is little to distinguish them. The predictions for an ellipsoidal fibre are consistent with the theoretical results of Eshelby [43]. However, cylindrical fibres have a substantial region near the end which is not being maximally stressed and which, therefore, contributes little to reinforcing the composite. Once again, changing q has little effect on the stress distributions in the cylindrical, the paraboloidal and ellipsoidal fibres. However, when E_f/E_m is large, reducing q has the effect of

concentrating stress towards the end of the tapered fibre, increasing it by up to an order of magnitude over the stress at the fibre centre for $q = 200$.

3.2 *Mode α and β*

Figure 4 a shows a sketch of σ_z versus distance along the fibre axis. The sketch is based on results obtained using FE analysis by Tripathi et al. [40]. The stress distribution represents a ‘snap-shot’ during the state of progression of deformation under an increasing applied load. In this sketch, there are three regions of stress distributions. Around the fibre end, i.e. zone 1, the stress distribution has been attributed to the effects of mode β . It was pointed out in section 2.3 that the onset of matrix failure (mode α) is initiated at the fibre end. Hence, in the early stages of failure, only two regions are observed and they correspond to mode α and elastic stress transfer [11,16]. Then the high stress concentration in the matrix around the fibre end influences interfacial debonding, resulting in mode β . It then follows that mode α recedes from this zone and migrates to zone 2. Regions such as zone 3 are free from high stress concentration so that the matrix remains elastic; hence elastic stress transfer dominates. Note that during fibre pull-out, i.e. mode γ (section 3.5), the regions of stress distribution (Figure 5 a) may also be attributed to the mixed mode feature discussed here.

In mode β , the distribution of σ_z is linear (Figure 4 a). This stress distribution is induced by frictional shear stress at the interface arising from relative motion between the deforming matrix and fibre (section 2.5) and has been predicted by the constant shear model of Kelly and Tyson [36]. Note also that a linear distribution of σ_z occurs in mode α (Figure 4 a); moreover, the corresponding interfacial shear stress is a constant. In this

case, since there is no interfacial debonding, this constant shear cannot be a result of relative motion between the matrix and fibre at the interface. A mathematical model developed by Landis and McMeeking explained that this was a result of the matrix behaving as a perfectly plastic material, i.e. the matrix yields under constant stress [19]. Predictions from their model agree well with results obtained from FE analysis [19].

3.3 *Mode γ*

Siviredin et al. [13] observed that the matrix deforms plastically from the debonded fibre end, EF (Figure 1). Consequently, a crack plane, originating from the debonded fibre end, initiates and propagates into the matrix. In their study, the crack plane described a frustrum and made an angle of less than 90° with respect to AF.

It may be assumed that the effects of a deforming plastic matrix around the fibre end region lead to distributions of σ_z and τ which are similar to those of mode α (Figure 4). In this case, σ_z increases linearly from zero at the fibre end over a distance until the point at which the region of plastic influence terminates; this linear region corresponds to a uniform τ .

3.4 *Plastic stress transfer*

FE models of plastic stress transfer in a uniform cylindrical fibre [21,30] are consistent with the results of theory [45,46] and experiment [17]. The axial tensile stress in the fibre rises linearly from zero, at the end, to a maximum value at the centre of the fibre; there is never any region resembling a plateau. The linear distribution of axial tensile stress is induced by frictional shear stress (section 3.2). For a conical fibre both FE models [21]

and theory [47] predict that the axial tensile stress is uniform. The stress distributions from the paraboloidal and ellipsoidal fibre lie between the two extremes of the cylinder and the cone [21,47]. The location of the maximum σ_z indicates a possible site of fracture. A cylindrical fibre is then expected to fracture at its centre but this is not the case for a fibre with a conical taper.

3.5 *Fibre pull-out*

Figure 5 a shows a sketch of σ_z versus distance, z , along the axis of a fibre. The sketch is based on results compiled from experiments, FE analysis and mathematical models [18,27,48]. The stress distribution is shown from the fibre end, $z = L'$, to the entry into the matrix crack plane, $z = 0$. The distribution of σ_z is divided into three zones. Bennett and Young [27] suggested that the linear stress distributions in zones 2 and 3 can be attributed to sliding when debonding at the interface (i.e. mode β) has occurred, whilst that in zone 1 is due to elastic stress transfer. In zones 2 and 3, they assigned different gradients corresponding to the different levels of friction experienced by the relative motion of the fibre and matrix during sliding. We suggest that the distribution of σ_z in zone 2 may be attributed to mode α rather than mode β ; the mixed mode proposed here has also been proposed in a different case, as explained in section 3.2. FE analysis carried out by Zhang et al. [18] predicted the distribution of σ_z in zone 3 to be a result of elastic stress transfer; the distribution of σ_z departs from that during initial loading (section 3.1) in that a peak value of σ_z is located at the point of transition from zone 2 to 1 which then rapidly decreases and plateaus out for most part of the length before decreasing to zero at the fibre end.

The corresponding distribution of τ is depicted in Figure 5 b. At zone 3, the FE analysis of Zhang et al. [18] predicted the distribution of τ as a result of elastic stress transfer. In this case, the distribution of τ departs from that during initial loading with an additional peak value of τ but is located at the point of transition from zone 2 to 3; this value is greater than that at $z = L'$.

3.6 Fibre fragmentation

Figure 6 a shows a sketch of σ_z versus z along the axes of fibre fragments lined up in series. The sketch is derived from results obtained by FE analysis reported by Rauchs et al. [17]; the predictions from FE analysis agree well with experiment. The sketch illustrates plastic stress transfer taking place; results of stress distributions obtained in some fibre fragmentation experiments [26,41,49] suggest that other processes such as elastic stress transfer, mode α or β may also be implicated. Stress distribution results from these studies [17,26,41,49] show two common features: (1) σ_z rises from the end of a cylindrical fibre fragment to a peak value at the fibre center and (2) a long fragment possesses a higher peak stress than a short fragment.

Figure 6 b shows the corresponding distribution of τ along the surface of these fibre fragments. Rauchs et al. demonstrated that if r_0 in all fragments had the same value and τ acting on all these fragments has the same magnitude, then the magnitude of σ_z depends on q . This is consistent with the constant shear model of Kelly & Tyson [36].

4 Discussions and conclusions

There have been many FE studies of short-fibre composites since the early work of Carrara & McGarry [8]. They have included studies of elastic stress transfer, plastic stress transfer, matrix yielding (mode α), interfacial debonding (mode β), matrix cracking (mode γ), fibre pull-out and fibre fragmentation. Indeed several models have been used to investigate the same problem. This duplication is inevitable and important because of the continuing improvements in the standard of FE modelling, as a result of better computer hardware, better specialist FE software and experience in the application of the technique to an increasingly wide range of problems. FE modelling of fibres which are not uniform cylinders [8,10,21] is providing insights into how fibre shape can influence the performance of composites. It is likely that increased computer speed will enable wider ranges of values for the parameters of FE models to be explored, leading to sensitivity analyses and making it possible to draw more general conclusions.

5 Acknowledgements

We thank the University of Aberdeen for the award of a postgraduate studentship to KLG, during the early stages of this work, and the Medical Research Council (UK) for the award of a Senior Fellowship to RMA.

References

1. Kelly A, MacMillan NH. Strong solids. 3rd ed.. Oxford: Oxford University Press, 1986.
2. Agarwal BD, Broutman LJ. Analysis and performance of fibre composites. 2nd ed.. New York: John Wiley & Sons, Inc., 1990.
3. Deleonardo G. Engineering analysis and simulation in General Electric's quality program. ANSYS Solutions 2000;2:32.
4. Reh S, Lethbridge P, Ostergaard D. Quality-based design with probabilistic methods. ANSYS Solutions 2000;2:20-22.
5. Meakin J, Hukins DWL. Replacing the nucleus pulposus of the intervertebral disk: prediction of suitable properties of a replacement material using finite element analysis. J Mater Sci Mater Med 2001;12:207-213.
6. Dar FH, Meakin JR, Aspden RM. Statistical methods in finite element analysis. J Biomech 2002;35:1155-1161.
7. ANSYS structural analysis guide. SAS IP, Inc., 2001.
8. Carrara AS, McGarry FJ. Matrix and interface stresses in a discontinuous fibre composite model. J Compos Mater 1968;2:222-243.
9. Owen DRJ, Lyness JF. Investigation of bond failure in fibre-reinforced materials by the finite element method. Fibre Sci Technol 1972;5:129-141.

10. Goh KL, Aspden RM, Mathias KJ, Hukins DWL. Finite element analysis of the effect of material properties and fibre shape on stresses in an elastic fibre embedded in an elastic matrix in a fibre composite material. Proc R Soc Lond A 2003;(in press).
11. Tripathi D, Chen FP, Jones FR. The effect of matrix plasticity on the stress fields in a single filament composite and the value of interfacial shear strength obtained from the fragmentation test. Proc R Soc Lond A 1996;452:621-653.
12. Nath RB, Fenner DN, Galiotis C. The progressional approach to interfacial failure in carbon reinforced composites: elasto-plastic finite element modeling of interface cracks. Composites Part A 2000;31:929-943.
13. Sirivedin S, Fenner DN, Nath RB, Galiotis C. Matrix crack propagation criteria for model short-carbon fibre/epoxy composites. Compos Sci Technol 2000;60:2835-2847.
14. Nairn JA. On the use of shear-lag methods for analysis of stress transfer unidirectional composites. Mech Mater 1997;26:63-80.
15. Wu W, Desaegeer M, Verpoest I, Varna J. An improved analysis of the stresses in a single-fibre fragmentation test .1. Two-phase model. Compos Sci Technol 1997;57:809-819.
16. Hayes SA, Lane R, Jones FR. Fibre/matrix stress transfer through a discrete interphase, Part 1: single-fibre model composites. Composites Part A 2001;32:379-389.

17. Rauchs G, Preuss M, Withers PJ. Micromechanical analysis of internal stress development during single-fibre fragmentation testing of Ti/SiCf. *Acta Mater* 2002;50:2477-2490.
18. Zhang X, Liu HY, Mai YW, Diao XX. On steady-state fibre pull-out - I - The stress field. *Compos Sci Technol* 1999;59:2179-2289.
19. Landis CM, McMeeking RM. A shear-lag model for a broken fibre embedded in a composite with a ductile matrix. *Compos Sci Technol* 1999;59:447-457.
20. Rosen BW. Mechanics of composite strengthening. In: *Fibre composite materials*. Ohio: American Society for Metals; 1965. p.37-75.
21. Goh KL, Aspden RM, Mathias KJ, Hukins DWL. Finite element analysis of the effect of fibre shape on stresses in an elastic fibre surrounded by a plastic matrix. *J Mater Sci* 2000;35:2493-2497.
22. Holmes DF, Chapman JA, Prockop DJ, Kadler KE. Growing tips of type I collagen fibrils formed in vitro are near-paraboloidal in shape, implying a reciprocal relationship between accretion and diameter. *Proc Natl Acad Sci* 1992;89:9855-9859.
23. DeVente JE, Lester GE, Trotter JA, Dahners LE. Isolation of intact collagen fibrils from healing ligament. *J. Electron Microsc* 1997;46:353-356.
24. Dibenedetto AT, Gurvich MR. Effect of friction between fiber and matrix on the fracture toughness of the composite interface. *J Mater Sci* 1998;33:4239-4248.

25. Whitney JM, Lawrence TD. Axisymmetric stress distribution around an isolated fibre fragment. In: Norman J. Johnston, editor. Toughened Composites, ASTM STP 937, Philadelphia: American Society for Testing and Materials, Philadelphia, 1987.
26. Nairn JA, Liu YC. Stress transfer into a fragmented anisotropic fibre through an imperfect interface. *Int J Solids Struct* 1997; 34: 1255-1281.
27. Bennett JA, Young RJ. The effect of fibre-matrix adhesion upon crack bridging in fibre reinforced composites. *Composites Part A* 1998;29A:1071-1081.
28. Cox HL. The elasticity and strength of paper and other fibrous materials. *J Appl Phys* 1952;3:72-79.
29. NAFEMS. A finite element primer. Glasgow: NAFEMS, 1992.
30. Goh KL. Fibre reinforcement in fibre composite materials: effect of fibre shape. PhD thesis, University of Aberdeen, Department of Biomedical Physics & Bioengineering, 2001.
31. Schuster DM, Scala E. The mechanical interaction of sapphire whiskers with a birefringent matrix. [Trans. TMS-AIME](#), 1964;230,1635-1640.
32. Gere JM, Timoshenko SP. *Mechanics of Materials*. 4th edition, Gloucester: Stanley Thornes (Publishers) Ltd, 1999.
33. Paipetis A, Galiotis C. Effect of fibre sizing on the stress transfer efficiency in carbon/epoxy model composites. *Composites Part A* 1996;27A:755-767.

34. Tenbusschen A, Selvadurai APS. Mechanics of the segmentation of an embedded fibre. 1. Experimental investigations. *J Appl Mech Trans ASME* 1995;62:87-97.
35. Ehrburger P, Donnet JB. Interface in composite materials. *Phil Trans R Soc Lond A* 1980;294:495-505.
36. Kelly A, Tyson WR. Tensile properties of fibre-reinforced metals: copper/tungsten and copper/molybdenum. *J Mech Phys Solids* 1965;13:329-350.
37. Bentur A, Mindess S. *Fibre Reinforced Cementitious Composites*. London:Elsevier Applied Science, 1990.
38. Hearle JWS, Lomas B, Cooke WD, Duerden IJ. *Fibre failure and wear of materials*. New York: Ellis Norwood, 1989.
39. Azangwe G, Mathias KJ, Marshall D. Macro and microscopic examination of the ruptured surfaces of anterior cruciate ligaments of rabbits. *J Bone Joint Surg Br* 2000;82B:450-456.
40. Tripathi D, Jones FR. Measurement of the load-bearing capability of the fibre/matrix interface by single-fibre fragmentation, *Compos Sci Technol* 1997;57:925-935.
41. Paipetis A, Galiotis C, Liu YC, Nairn JA. Stress transfer from the matrix to the fibre in a fragmentation test: Raman experiments and analytical modeling. *J Compos Mater* 1999;33:377-399.

42. Young RJ, Thongpin C, Stanford JL, Lovell PA. Fragmentation analysis of glass fibres in model composites through the use Raman spectroscopy. *Composites Part A* 2002;32:253-269.
43. Eshelby JD. The determination of the elastic field of an ellipsoidal inclusion and related problems. *Proc R Soc Lond A* 1957;241:376-396.
44. Galiotis C, Young RJ, Yeung PHJ & Batchelder DN. The study of model polydiacetylene/epoxy composites part 1 the axial strain in the fibre. *J Mater Sci* 1984;19:3640-3648.
45. Aspden RM. Fibre stress and strain in fibre-reinforced composites. *J Mater Sci* 1994;29:1310-1318.
46. Goh KL, Hukins DWL, Aspden RM. Critical length of collagen fibrils in extracellular matrix. *J Theor Biol* 2003; 223:259-261.
47. Goh KL, Aspden RM, Mathias KJ, Hukins DWL. Effect of fibre shape on the stresses within fibres in fibre-reinforced composite materials. *Proc R Soc Lond A* 1999; 455:3351-3361.
48. Bannister DJ, Andrews MC, Cervenka AJ, Young RJ. Analysis of the single-fibre pull-out test by means of Raman spectroscopy: Part II. Micromechanics of deformation for an aramid/epoxy system. *Compos Sci Technol* 1995;53:411-421.

49. Beyerlein IJ, Phoeni L. Stress profiles and energy release rates around fibre breaks in a lamina with propagating zones of matrix yielding and debonding. *Compos Sci Technol* 1997;57:869-885.

Captions

Figure 1 Sketch of a 3D axisymmetric FE model represented in 2D for an upper right quadrant. The model is described using cylindrical polar coordinates. The axis of the fibre defines the z -axis. The shaded region, OAFE, represents a fibre having a length of $2L$ and is entirely embedded in a matrix material (unshaded region); both fibre and matrix materials are homogeneous and isotropic. The FE model possesses both axisymmetry (about OD) and mirror symmetry (about OB) so only a quarter of the model is needed for the analysis. The mesh contains quadrilateral elements. Larger elements are assigned where little changes in stresses are expected, e.g. at regions in the matrix and fibre which are far away from the fibre end, and progressively smaller elements are introduced where the stress gradient gets larger, such as around the fibre ends. In practice, many more elements are used in the mesh.

Figure 2 Far-field analysis for convergence of distributions of axial stress, σ_z/σ_c , versus fractional distance, Z , along the (a) fibre axis and (b) matrix surface as r_m/r_o increases. Further details on nomenclature are given in section 1. Stress distributions are shown for $r_m = 10r_o$ (dot), $50r_o$ (circle), $100r_o$ (asterisk), $200r_o$ (diamond), $750r_o$ (triangle); not shown are those corresponding to $1000r_o$, which was the maximum matrix radius used for testing for convergence. These results were obtained using $E_f/E_m = 10^4$ and $q = 1000$; similar results were obtained for the other extreme values of E_f/E_m and q . At low values of r_m/r_o , i.e. the matrix surface being nearer to the fibre, almost all the load is found to be carried in the fibre [49] hence in (b) we have smaller value of σ_z/σ_c values along BF' as compared to F'C (Figure 1). The results for this figure are taken from reference [10].

Figure 3 Elastic stress transfer. Graph of axial stress, σ_z/σ_c , versus fractional distance, Z , along the half-length of a cylindrical fibre with values of $(E_f/E_m, q)$ of $(10^4, 1000)$, $(10^4, 200)$, $(50, 1000)$ and $(50, 200)$; these are represented as dots, circles, asterisks and diamonds, respectively, connected by solid lines. Further details on nomenclature are given in section 1. The results for this figure are taken from reference [10].

Figure 4 Sketches of distributions of (a) fibre axial stress, σ_z , and (b) interfacial shear stress, τ , versus distance along the half-length of a cylindrical fibre, z , based on FE analysis carried out by Tripathi and Jones [40]. Indicated on these sketches are zones corresponding to mode β , mode α and elastic stress transfer.

Figure 5 Sketches of distributions of (a) fibre axial stress, σ_z , and (b) interfacial shear stress, τ , versus distance along the fibre axis, z , during pull-out of a cylindrical fibre, based on results obtained from [18,27,48]. Here, the point of application of the applied stress is at $z = 0$; the fibre end is at $z = L'$. Indicated on these sketches are zones corresponding to mode β , mode α and elastic stress transfer.

Figure 6 Sketches of distributions of (a) fibre axial stress, σ_z , and (b) interfacial shear stress, τ , versus distance along the fibre axis, z , of fibre fragments, based on FE analysis carried out by Rauchs et al. [17]. Here, L_1 , L_2 and L_3 represents the lengths of the fibre fragments.

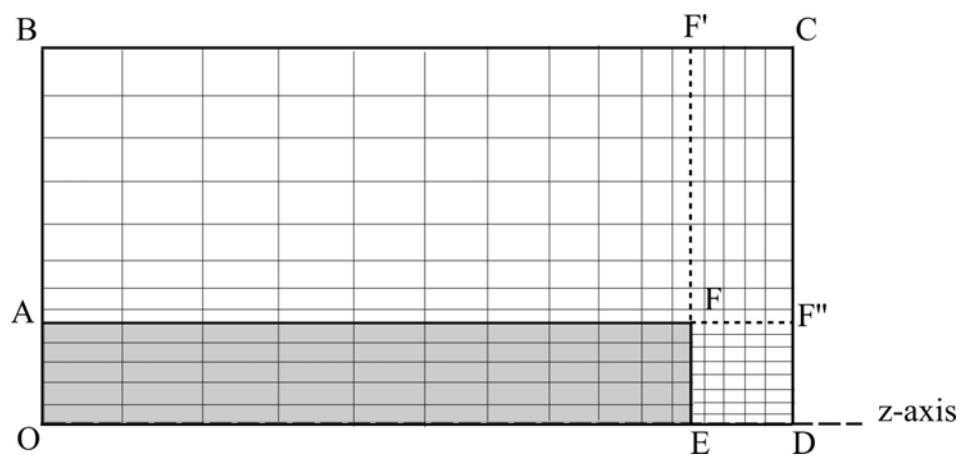


Figure 1

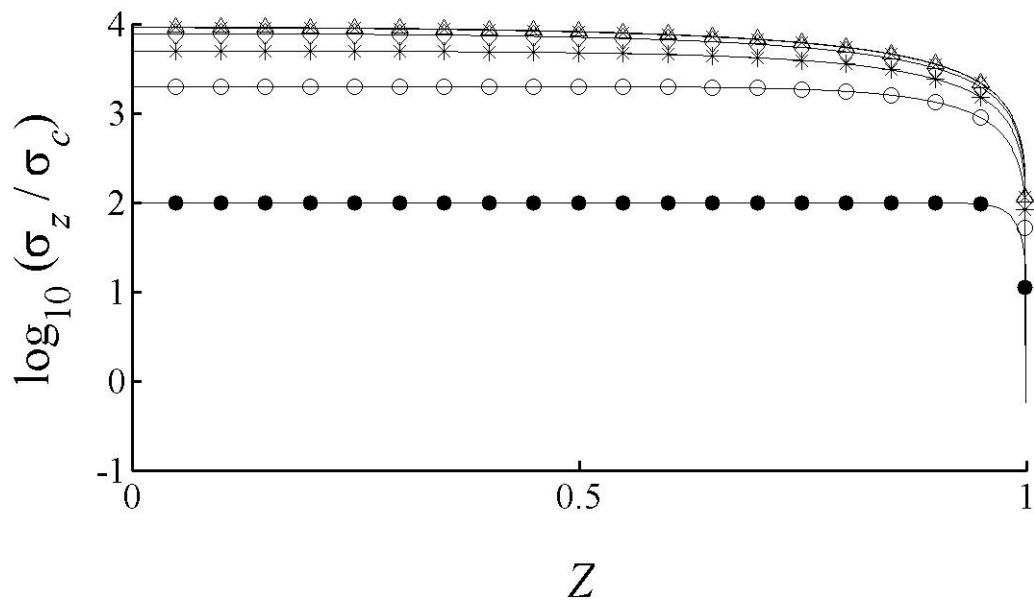


Figure 2 a

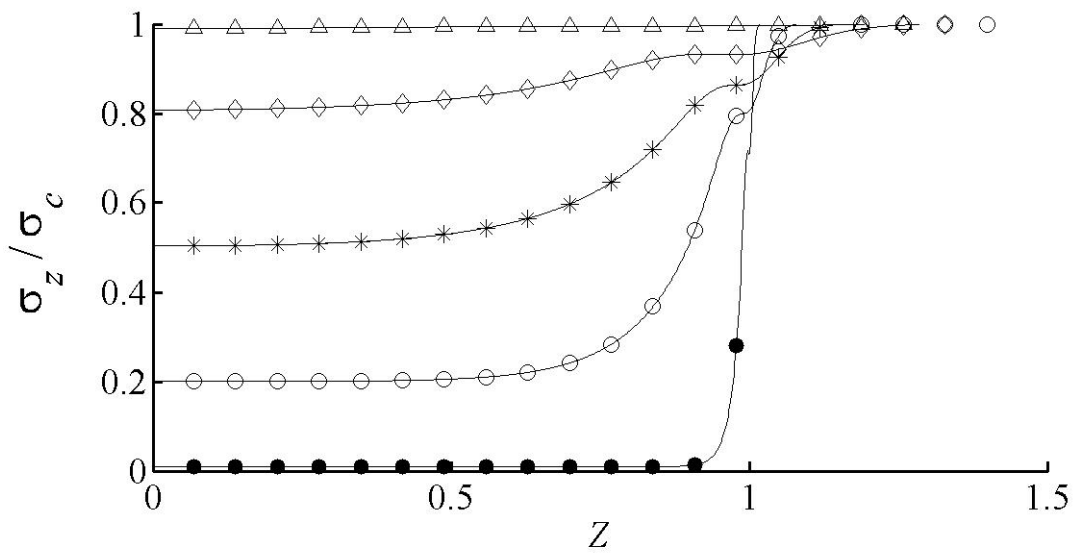


Figure 2 b

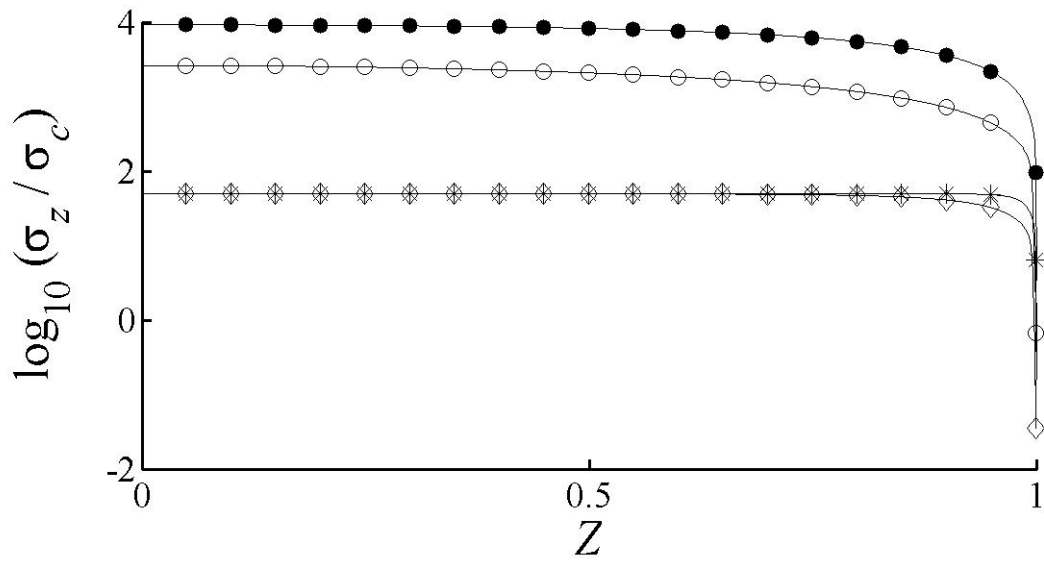


Figure 3

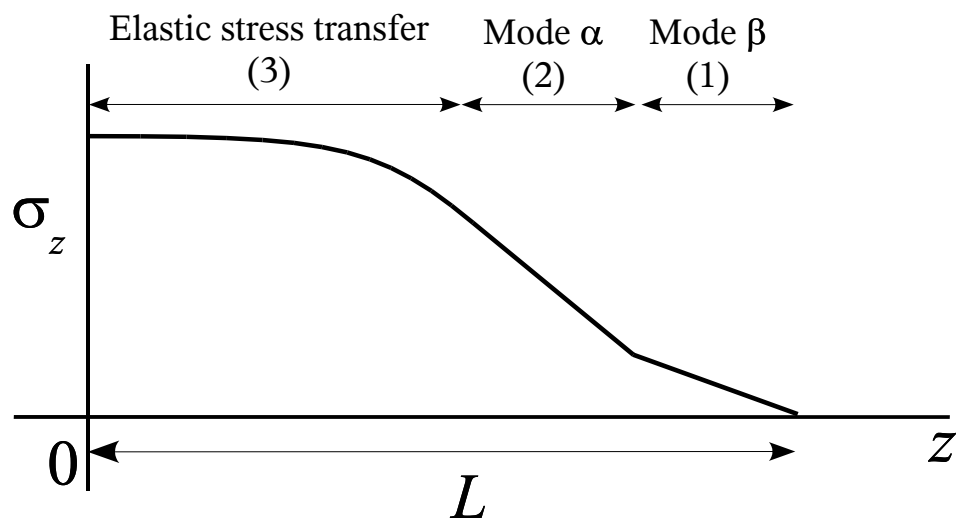


Figure 4 a

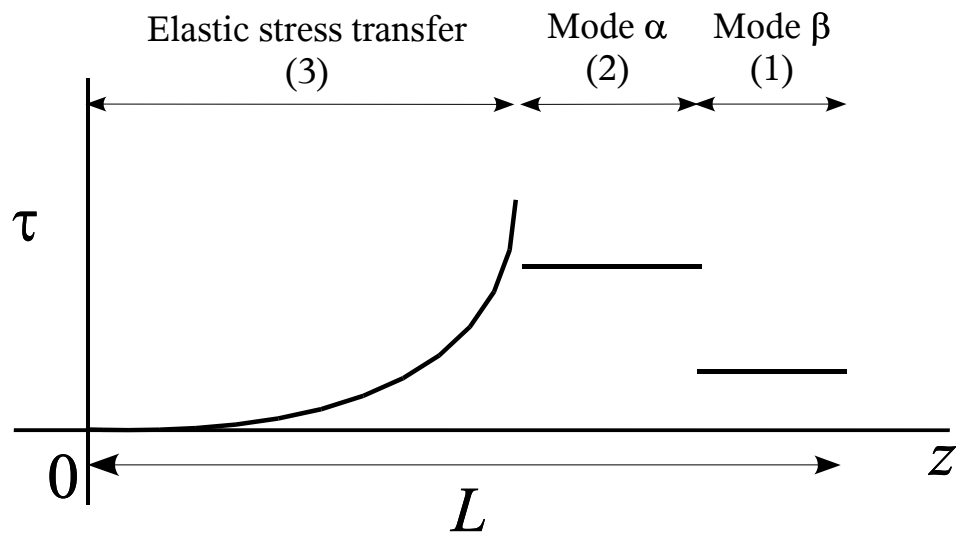


Figure 4 b

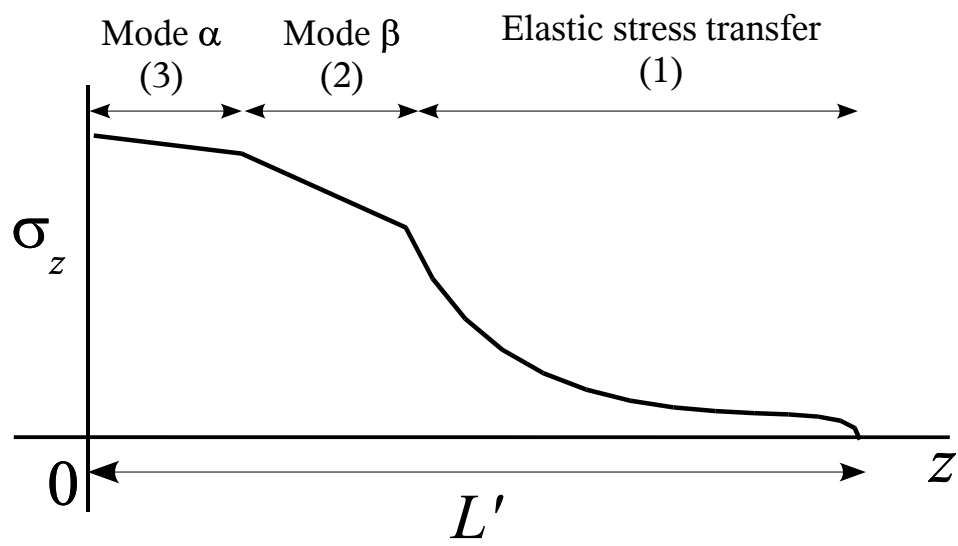
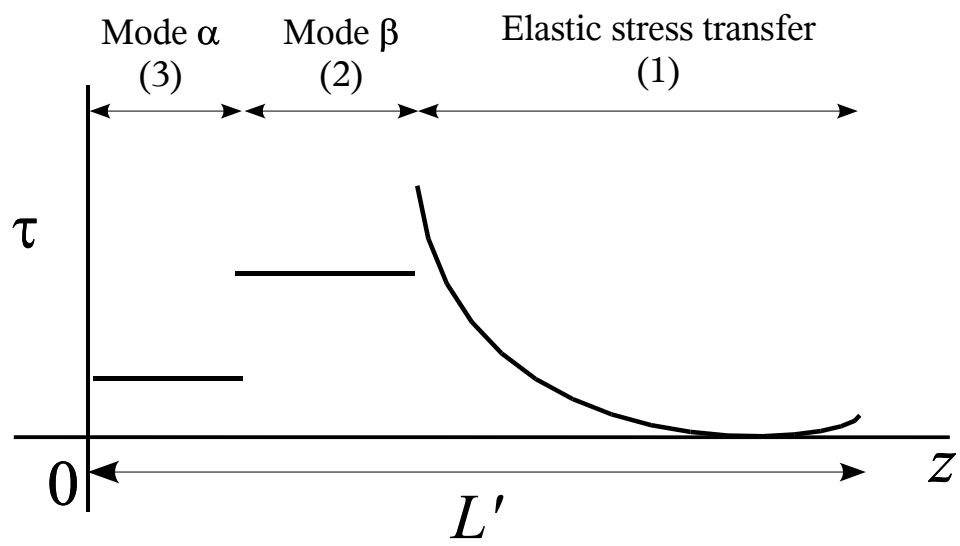


Figure 5 a



[Figure 5 b](#)

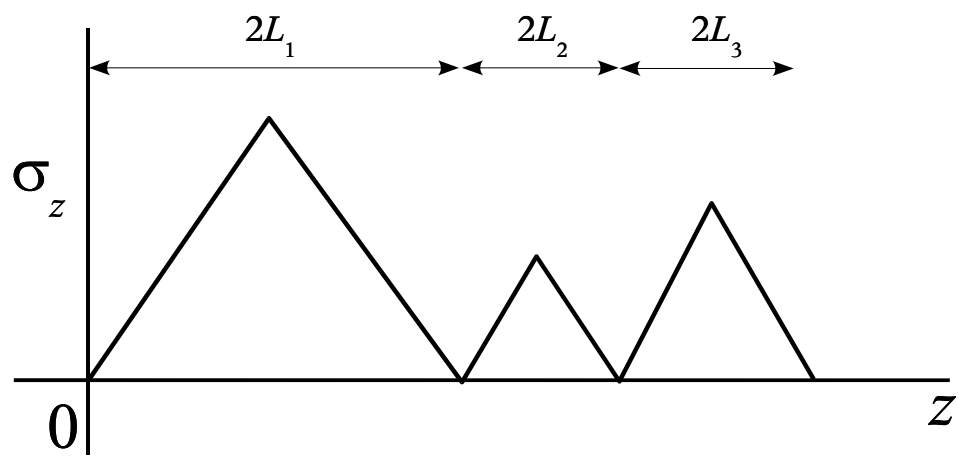


Figure 6 a

